




Article

Investigating Natural Product Inhibitors of IKK α : Insights from Integrative In Silico and Experimental Validation

Muhammad Yasir ¹, Jinyoung Park ¹, Eun-Taek Han ², Jin-Hee Han ² , Won Sun Park ³, Jongseon Choe ⁴ 
and Wanjoon Chun ^{1,*} 

¹ Department of Pharmacology, Kangwon National University School of Medicine, Chuncheon 24341, Republic of Korea; yasir.khokhar1999@gmail.com (M.Y.); jinyoung0326@kangwon.ac.kr (J.P.)

² Department of Medical Environmental Biology and Tropical Medicine, Kangwon National University School of Medicine, Chuncheon 24341, Republic of Korea; ethan@kangwon.ac.kr (E.-T.H.); han.han@kangwon.ac.kr (J.-H.H.)

³ Department of Physiology, Kangwon National University School of Medicine, Chuncheon 24341, Republic of Korea; parkws@kangwon.ac.kr

⁴ Department of Microbiology and Immunology, Kangwon National University School of Medicine, Chuncheon 24341, Republic of Korea; jchoe@kangwon.ac.kr

* Correspondence: wchun@kangwon.ac.kr; Tel.: +82-33-250-8853

Abstract: Nuclear factor- κ B (NF- κ B) signaling plays a pivotal role in regulating immune responses and is strongly implicated in cancer progression and inflammation-related diseases. The inhibitory κ B kinases (IKKs), particularly IKK α , are central to modulating NF- κ B activity, with distinct roles in the canonical and non-canonical signaling pathways. This study investigates the potential of selectively targeting IKK α to develop novel therapeutic strategies. A receptor–ligand interaction pharmacophore model was generated based on the co-crystallized structure of IKK α , incorporating six key features, two hydrogen bond acceptors, two hydrogen bond donors, one hydrophobic region, and one hydrophobic aromatic region. This model was used to virtually screen a diverse natural compound library of 5540 molecules, yielding 82 candidates that matched the essential pharmacophore features. Molecular docking and molecular dynamics simulations were subsequently employed to evaluate binding conformations, stability, and dynamic behavior of the top hits. The end-state free energy calculations (gmx_MMPBSA) further validated the interaction strength and stability of selected compounds. To experimentally confirm their inhibitory potential, key compounds were tested in LPS-stimulated RAW 264.7 cells, where they significantly reduced IKK α phosphorylation. These findings validate the integrative computational-experimental approach and identify promising natural compounds as selective IKK α inhibitors for further therapeutic development in cancer and inflammatory diseases.

Keywords: IKK α ; IKK β ; NF- κ B; inflammation; pharmacophore modeling; molecular docking; molecular dynamic simulation; RAW 264.7 cells



Academic Editor: Katarína Bauerová

Received: 20 March 2025

Revised: 17 April 2025

Accepted: 30 April 2025

Published: 2 May 2025

Citation: Yasir, M.; Park, J.; Han, E.-T.; Han, J.-H.; Park, W.S.; Choe, J.; Chun, W. Investigating Natural Product Inhibitors of IKK α : Insights from Integrative In Silico and Experimental Validation. *Molecules* **2025**, *30*, 2025. <https://doi.org/10.3390/molecules30092025>

Copyright: © 2025 by the authors. Licensee MDPI, Basel, Switzerland. This article is an open access article distributed under the terms and conditions of the Creative Commons Attribution (CC BY) license (<https://creativecommons.org/licenses/by/4.0/>).

1. Introduction

Nuclear factor- κ B (NF- κ B) transcription factors are vital regulators of both the innate and adaptive immune responses, and they also play a central role in the development and progression of cancer [1–3]. These factors contribute to several critical processes, such as enabling preneoplastic and malignant cells to evade apoptosis, promoting tumor angiogenesis, and invasiveness. Because of these functions, the signaling pathways that

activate NF- κ B complexes present promising targets for developing new chemotherapeutic strategies [2,4–7].

The activation of NF- κ B is primarily regulated by inhibitory κ B kinases (IKKs), which become overactive when cellular homeostasis is disrupted [8,9]. This overactivity is marked by increased constitutive activity of IKK α and IKK β , leading to elevated NF- κ B expression and its subsequent translocation into the nucleus [10]. IKKs function as upstream regulators of NF- κ B activity by existing as either homo- or heterodimers, bound to inhibitory proteins called I κ Bs. In the canonical pathway, IKK activation leads to the phosphorylation, ubiquitination, and proteolytic degradation of I κ Bs, which allows NF- κ B complexes to migrate into the nucleus and activate specific gene expression [11–14]. On the other hand, the non-canonical pathway involves the phosphorylation and processing of the NF- κ B precursor protein p100, which then generates p52/RelB dimers that drive the expression of a distinct set of genes [15–19].

Research has shown that IKK α and IKK β play distinct but essential roles in regulating global NF- κ B signaling. IKK β is primarily involved in the canonical pathway, where it activates p65 RelA–p50 heterodimers. Its inhibition has been shown to reduce pro-inflammatory gene expression in various cell types, which is crucial since many pro-inflammatory molecules contribute to cancer progression [15,20–22]. Although IKK α plays a less prominent role in the canonical pathway, it is crucial in the non-canonical pathway. IKK α catalyzes the phosphorylation and processing of p100, generating p52/RelB dimers, which activate a specific subset of genes [15,23].

In recent years, much attention has been given to selectively inhibiting IKK α . Over the last two decades, several IKK α inhibitors have been discovered, mainly for the treatment of inflammatory conditions [24–28]. However, recent findings suggest that inhibiting IKK β can lead to significant toxic effects, including inflammatory skin diseases and increased sensitivity of the colonic epithelium to various types of damage [28–30]. In contrast, IKK α inhibition seems to offer a safer and more targeted approach. For example, a natural compound called noraristeromycin (NAM) has been found to selectively inhibit IKK α . NAM prevents the phosphorylation and degradation of I κ B α after TNF α stimulation, and it also blocks the phosphorylation of the NF- κ B subunit p65 [27,31,32]. These findings highlight the potential of NAM and other IKK α inhibitors as therapeutic agents.

Given the growing body of evidence supporting the critical role of IKK α in cancer, particularly in prostate, breast, and pancreatic cancers, there is an urgent need for selective IKK α inhibitors [32,33]. These inhibitors would not only provide deeper insights into the role of IKK α in cancer development and progression but also offer a promising strategy for developing targeted therapies for cancers where IKK α is implicated in tumor growth and metastasis. However, natural products against IKK α have not been widely explored. Therefore, filling out the remaining gaps, this study aims to identify promising lead compounds for targeted IKK α inhibition from the pool of natural compounds, thus proposing Valyltyrosine, Noricaritin, Caffeoyltryptophan, and Leonurine as potent drug candidates (Figure 1).

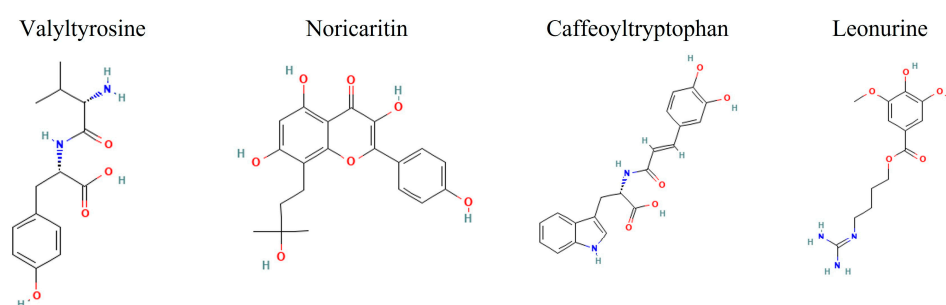


Figure 1. The 2D images of the screened candidate compounds against IKK α .

2. Results and Discussion

2.1. Pharmacophore Modeling

One of the major challenges in drug discovery is addressing the side effects caused by the non-selective action of compounds, which can lead to unintended interactions with off-target proteins [34,35]. To mitigate this issue, pharmacophore modeling emerges as a powerful strategy. By focusing on the essential features required for selective binding, pharmacophore modeling enables the identification and screening of compounds that closely match the active binding pocket of a target protein, thereby improving specificity and reducing off-target effects [36–38].

Previously, pharmacophore studies for IKK β had shown some promising results and a number of potential inhibitors were suggested against the IKK β [39,40]. However, a recent study suggested that inhibiting IKK β can lead to toxic effects such as inflammatory skin diseases and increased sensitivity of the colonic epithelium [28–30].

The resulting pharmacophore model of this study for IKK α was critical for binding efficacy and selectivity. A total of 10 pharmacophore models were predicted by the RLIPG approach in Discovery Studio (Supplementary data Table S1); therefore, the top pharmacophore was chosen for further library screening. The model included two hydrogen-bond acceptors (green), two hydrogen-bond donors (magenta), a hydrophobic region (cyan), and a hydrophobic aromatic region (blue). These features correspond to functional groups on the ligand that can form strong and specific interactions with complementary regions of the target protein. Additionally, the model incorporated excluded volume areas (gray), representing sterically inaccessible regions that restrict the binding of non-specific compounds (Figure 2).

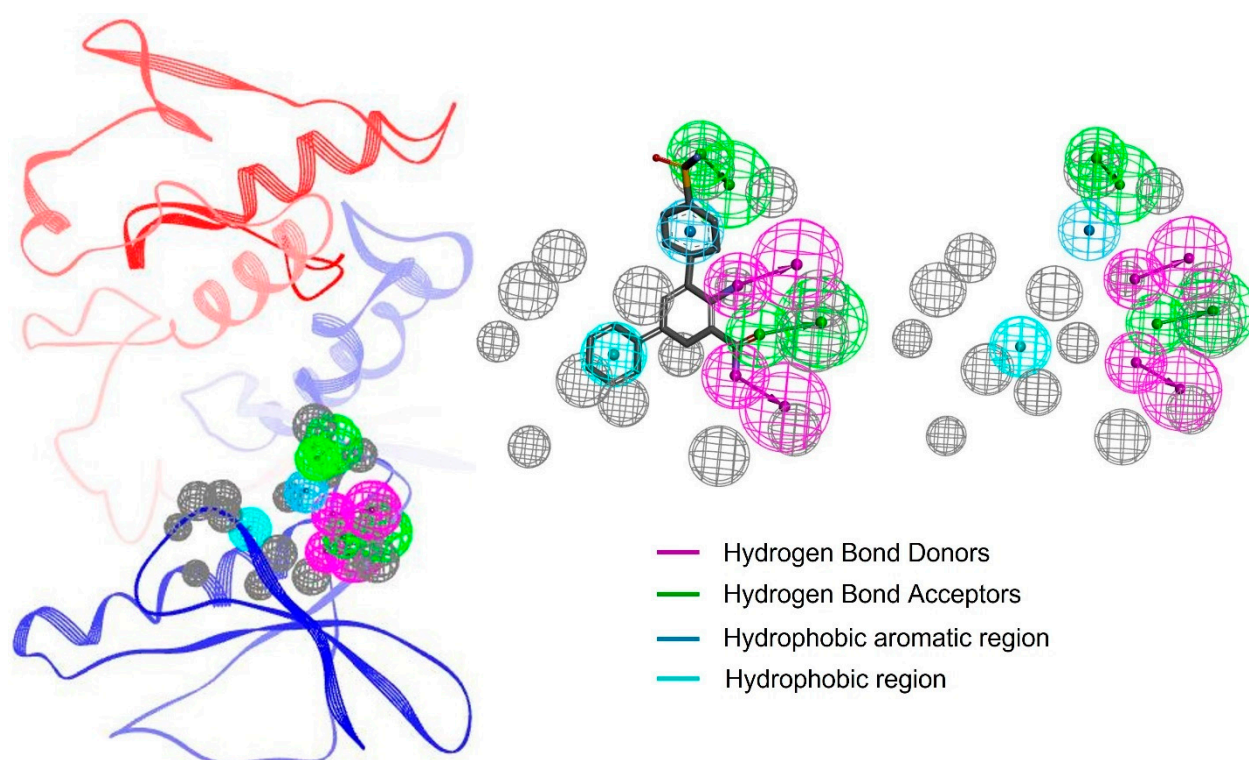


Figure 2. The pharmacophore features of the protein–ligand complex. Each feature is highlighted in a different color. The excluded volume areas are colored as grey.

The hydrogen-bond acceptors and donors play a pivotal role in stabilizing the ligand within the binding pocket, forming strong electrostatic interactions with complementary residues on IKK α . These interactions are complemented by the hydrophobic region, which

enhances binding affinity by interacting with nonpolar residues in the protein's active site. The inclusion of excluded volume features ensures that only compounds with an optimal size and shape can align with the pharmacophore, further refining selectivity [30,41,42].

By integrating critical interaction features such as hydrogen bond donors and acceptors, hydrophobic regions, and excluded volumes, the pharmacophore model serves as a precise blueprint for identifying ligands with high binding specificity. This model not only facilitates efficient virtual screening but also enhances lead optimization by filtering out compounds unlikely to interact with IKK α 's active site. As a result, the selected hits are more likely to exhibit selective binding to IKK α while minimizing interactions with structurally similar kinases, thereby reducing the risk of off-target effects and potential toxicity. This strategic design approach plays a crucial role in improving the quality and therapeutic relevance of the identified inhibitors.

2.2. Molecular Docking

The CDocker module in Discovery Studio evaluates the binding affinity and interaction between small molecules and a target protein by calculating two key energy parameters: CDocker Energy and CDocker Interaction Energy. CDocker Energy (measured in kcal/mol) reflects the total internal and binding energy of the ligand–protein complex. A lower CDocker Energy value indicates a more stable and energetically favorable binding conformation, signifying stronger interactions, whereas the CDocker Interaction Energy (also in kcal/mol) measures the direct interaction strength between the ligand and the protein [43–45]. Highly negative interaction energy values suggest that the compound forms strong interactions with the active site residues of IKK α . Out of the 82 pharmacophore screened compounds, 22 compounds were excluded during the ligand preparation step by Discovery Studio's default settings. The Discovery studio has built an exclusion criteria for the compounds that failed to meet structural or chemical requirements necessary for molecular docking, such as having undefined valency, missing atoms, unresolved stereochemistry, or failure to generate a valid 3D conformation during minimization. Consequently, the remaining 60 well-prepared compounds were selected for molecular docking to the active binding site of IKK α (Supplementary data Table S2).

To provide a comparative docking performance of the screened compounds, three IKK known inhibitors, BMS-345541, IMD-2560, and TPCA-1, were included as reference compounds. BMS-345541 exhibited a CDocker energy of -35.3389 kcal/mol and the strongest interaction energy of -50.2900 kcal/mol, supporting its high interaction role but less overall docking score. IMD-2560 showed a moderate binding affinity to IKK α with a CDocker energy of -32.9077 kcal/mol and interaction energy of -34.2859 kcal/mol. TPCA-1, another IKK inhibitor, demonstrated the weakest binding with a CDocker energy of -29.1605 kcal/mol and interaction energy of -31.641 kcal/mol. These reference values provided a comparative framework, highlighting that several natural compounds identified displayed equal or superior binding characteristics.

Among the top 10 screened compounds (Figure 3), Valyltyrosine emerged as the top-ranked compound with the most favorable CDocker energy (-47.7948 kcal/mol) and a strong interaction energy (-44.1606 kcal/mol), indicating a potentially stable binding configuration with the target. Noricaritin followed, exhibiting CDocker energy of -40.1424 kcal/mol and a stronger interaction energy of -46.5164 kcal/mol, suggesting its binding is more dependent on specific interactions. Caffeoyltryptophan, with CDocker energy of -38.5329 kcal/mol and interaction energy of -38.7883 kcal/mol, showed balanced binding properties (Table 1). Leonurine also displayed a relatively high CDocker energy (-35.8290 kcal/mol) but the lowest interaction energy (-48.1231 kcal/mol) among the group, implying robust intermolecular interactions despite its overall binding energy. Com-

pounds like Rhamnetin and Padmatin showed comparable CDocker energies (-35.3055 and -33.0318 kcal/mol, respectively) but differing interaction energies (-40.3473 and -43.3144 kcal/mol), highlighting differences in their binding efficiency. Other compounds, including Prudomestin, Wushanicaritin, Rhamnocitrin, and Blumeatin B, displayed progressively less CDocker energies, yet their interaction energies suggested the presence of meaningful binding interactions, as summarized in Table 1.

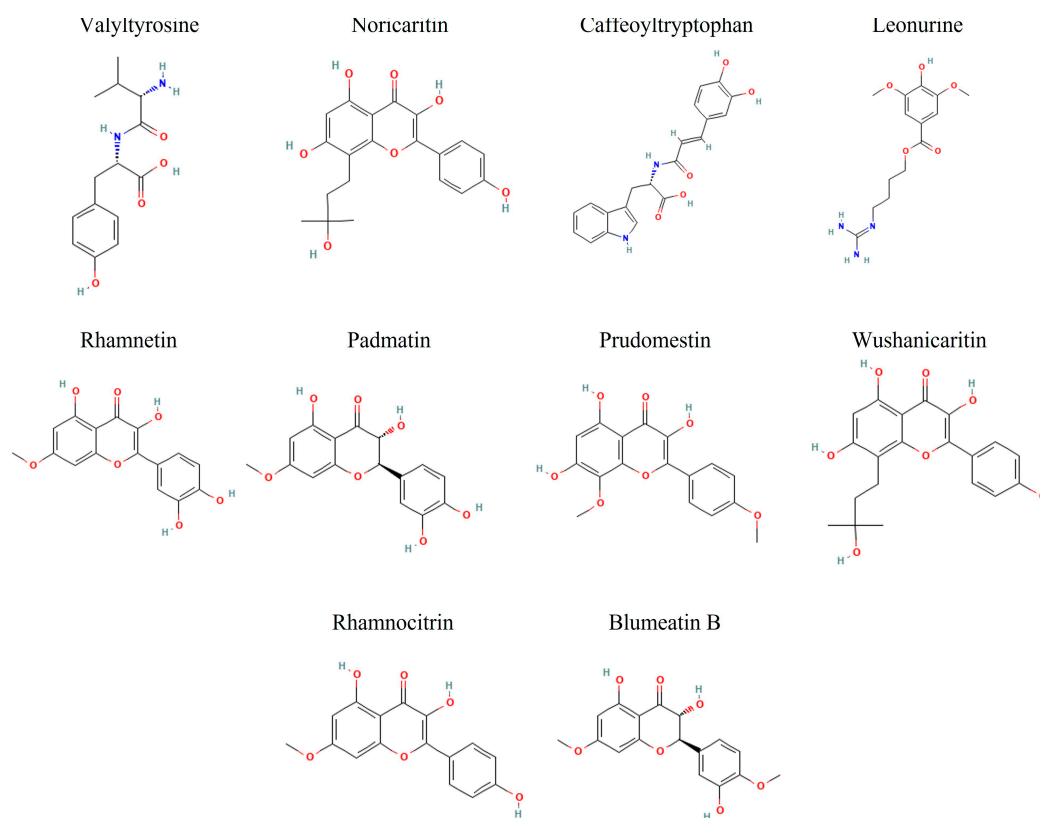


Figure 3. The 2D representation of the top 10 docked compounds against IKK α .

Table 1. The docking energy values of the top 10 docked compounds, ranked considering the overall CDocker energy values.

| Sr No | Compounds | CDocker Energy (kcal/mol) | CDocker Interaction Energy (kcal/mol) |
|-------|----------------------|---------------------------|---------------------------------------|
| 1 | Valyltyrosine | -47.7948 | -44.1606 |
| 2 | Noricaritin | -40.1424 | -46.5164 |
| 3 | Caffeoilyltryptophan | -38.5329 | -38.7883 |
| 4 | Leonurine | -35.8290 | -48.1231 |
| 5 | BMS-345541 (Ref) | -35.3389 | -50.2900 |
| 6 | Rhamnetin | -35.3055 | -40.3473 |
| 7 | Padmatin | -33.0318 | -43.3144 |
| 8 | IMD-2560 (Ref) | -32.9077 | -34.2859 |
| 9 | Prudomestin | -32.3987 | -42.4406 |
| 10 | Wushanicaritin | -32.3714 | -46.2998 |
| 11 | Rhamnocitrin | -31.4653 | -38.4445 |
| 12 | Blumeatin B | -30.1299 | -42.6128 |
| 13 | TPCA-1 (Ref) | -29.1605 | -31.641 |

Hypothetically, compounds with lower CDocker energy generally correlate with better stability within the binding pocket. However, interaction energy variations may indicate differences in the strength and nature of intermolecular forces, such as hydrogen bonding, hydrophobic interactions, or ionic contacts. Overall, Valyltyrosine, Noricaritin, Caffeoyltryptophan, Leonurine, and Rhamnetin manifested the most favorable docking profiles. Valyltyrosine is a dipeptide commonly found in fermented soy products and certain protein-rich plant sources. Noricaritin is a flavonoid derivative predominantly isolated from species within the *Carthamus* genus (e.g., *Carthamus tinctorius*, commonly known as safflower), which has been traditionally used in Chinese medicine. Caffeoyltryptophan is an esterified amino acid compound identified in several plant-based foods, especially those rich in hydroxycinnamic acids and indole-containing compounds, such as coffee beans and legumes. Leonurine is an alkaloid found in *Leonurus japonicus* (motherwort), a plant widely used in East Asian traditional medicine for its anti-inflammatory and cardioprotective properties. Rhamnetin, a naturally occurring flavonoid, is found in several medicinal plants, including *Sophora japonica* and Clove (*Syzygium aromaticum*), and has been studied for its antioxidant and anti-inflammatory effects. Moreover, Padmatin, Prudomestin, Prudomestin, Wushanicaritin, Rhamnocitrin, and Blumeatin B also showed the inhibitory potential against the target protein given their combination of strong CDocker and CDocker interaction energies. However, the real-time stability needs to be explored for these compounds in molecular dynamics simulations.

2.3. Molecular Docking Interactions

The molecular docking interaction analysis for the top 10 screened compounds was conducted to evaluate their interactions within the active site of the target protein. The results revealed that all compounds successfully docked within the active region and formed significant intermolecular interactions, including hydrogen bonds and salt bridges. While hydrophobic interactions were also observed (Supplementary data Figure S1), the primary focus was on stronger interactions that contribute significantly to binding stability, so only hydrogen bonds and salt bridges were discussed deeply. Valyltyrosine exhibited strong binding, forming one hydrogen bond and one salt bridge with bonding distances of 2.23 Å and 1.83 Å, respectively, suggesting highly stable interactions. Noricaritin, which ranked second in molecular docking energy after Valyltyrosine, demonstrated a notable interaction profile by forming three hydrogen bonds (one with Thr23 and two with Cys98) indicating robust anchoring within the active site. Caffeoyltryptophan displayed a complex interaction network, engaging with multiple amino acids, including Asp102, Cys98, Gly22, and Lys146. Its bonding distances ranged from 1.85 Å to 2.74 Å, highlighting its vast binding mechanism. Leonurine, ranked fourth, formed a single hydrogen bond with Arg20 at distances of 1.83 Å and 2.37 Å, implying a reliance on electrostatic stabilization. Similarly, compounds such as Rhamnetin, Padmatin, and Rhamnocitrin each formed two hydrogen bonds, targeting key residues like Cys98 and Thr23, while maintaining moderate binding affinities (Table 2).

In contrast, Prudomestin, Wushanicaritin, and Blumeatin B formed only one hydrogen bond each, focusing primarily on key residues such as Cys98 and Glu148. Despite having fewer interactions, the precise targeting of critical residues by these compounds suggests their potential as inhibitors. For instance, Wushanicaritin's interaction with Cys98 at 2.11 Å indicates a strong binding focus on this residue. Among the compounds docked, the graphical depiction of the interactions of the top five compounds is manifested in Figure 4; the remaining five compounds' interactions are manifested in the Supplementary data Figure S2.

A graphical depiction of the interactions formed during the molecular docking analysis is represented below.

Table 2. The hydrogen bonds and the salt bridges observed in the molecular docking interaction analysis; salt bridges are denoted with bold representation, whereas hydrogen bonds are depicted without emphasis.

| Compounds | Interacting Residues | Binding Distances |
|--------------------|----------------------|-------------------|
| Valyltyrosine | Gly22 | 2.23 Å |
| | Asp102 | 1.83 Å |
| Noricaritin | Thr23 | 2.05 Å |
| | Cys98 | 1.98 Å, 1.85 Å |
| Caffeoyltryptophan | Asp102 | 2.09 Å |
| | Cys98 | 1.85 Å |
| | Gly22 | 2.74 Å |
| | Lys146 | 1.89 Å |
| Leonurine | Arg20 | 1.83 Å, 2.37 Å |
| Rhamnetin | Cys98 | 2.41 Å |
| | Thr23 | 2.16 Å |
| Padmatin | Arg20 | 1.87 Å |
| | Glu148 | 1.97 Å |
| Prudomestin | Cys98 | 2.34 Å, 2.01 Å |
| Wushanacaritin | Cys98 | 2.11 Å |
| Rhamnocitrin | Thr23 | 2.19 Å |
| | Cys98 | 2.28 Å |
| Blumeatin B | Glu148 | 1.97 Å |

The bolded amino acid residues represent the salt bridges and the length of the salt bridges.

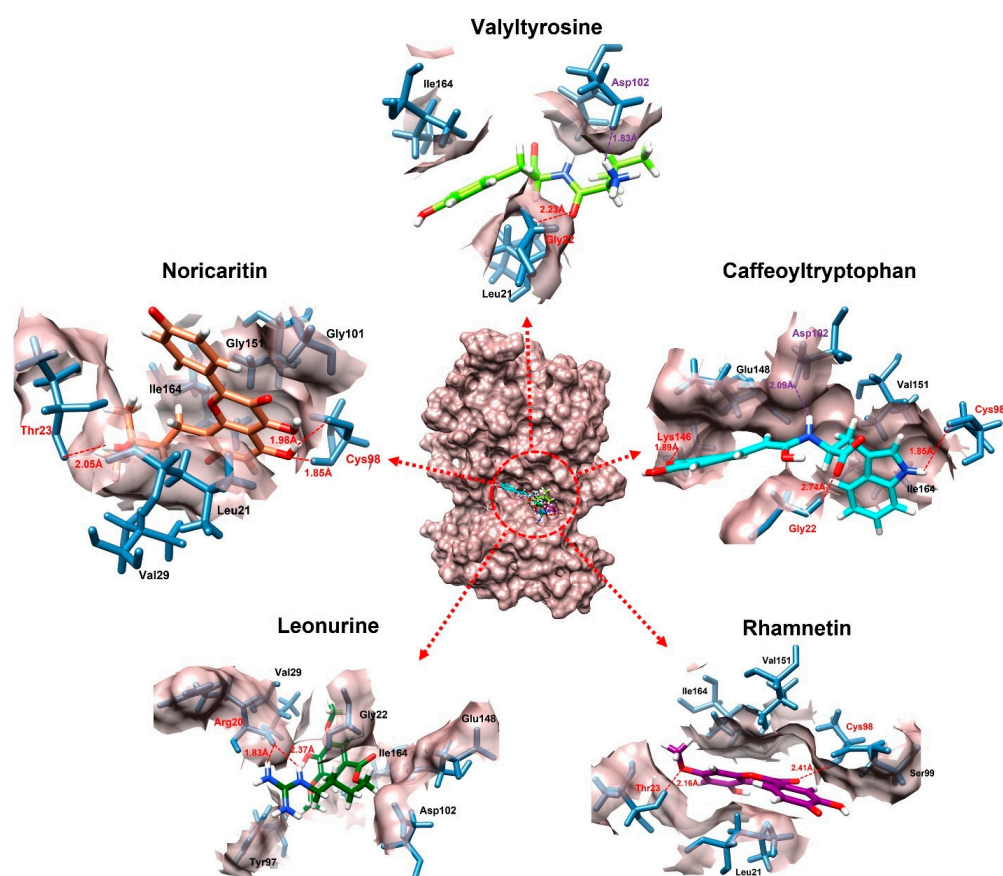


Figure 4. The interactions of the top five docked compounds against the active region of the IKK α . The salt bridges are colored as purple, hydrogen bonds are colored red, while the amino acids interacting hydrophobically are colored as black.

2.4. Molecular Dynamic Simulation

To further evaluate the stability of the top 10 screened compounds against IKK α in comparison with BMS-345541 as a reference, 100 ns molecular dynamics (MD) simulations were performed using GROMACS. BMS-345541 was chosen based on its high performance in molecular docking studies, while the MD results of the other two reference compounds have been provided in the Supplementary data Figure S3. This analysis provided a dynamic assessment to confirm the potential of these compounds as effective inhibitors of IKK α .

2.4.1. Root Mean Square Deviation Analysis

A comprehensive RMSD (Root Mean Square Deviation) analysis was performed for the top 10 screened compounds to evaluate their real-time stability when complexed with the target protein. The RMSD results revealed that the top five screened compounds (Valyltyrosine, Noricaritin, Caffeoilytryptophan, Leonurine, and Rhamnetin) exhibited highly stable RMSD profiles throughout the molecular dynamics (MD) simulation as compared to BMS-345541, indicating consistent binding and minimal structural deviations (Figure 5). These findings align well with their superior docking scores, suggesting that their initial binding conformations remained stable throughout the simulation. Among the remaining five compounds, Wushanicaritin and Blumeatin B also displayed relatively stable RMSD values, albeit with slightly higher fluctuations compared to the top five compounds. Notably, Blumeatin B exhibited significant instability at the start of the MD simulation, as evidenced by a highly fluctuating RMSD profile during the initial phase. However, after 21 ns, the RMSD values began to stabilize, reflecting eventual equilibrium and suggesting that the compound underwent conformational adjustments before settling into a stable binding state.

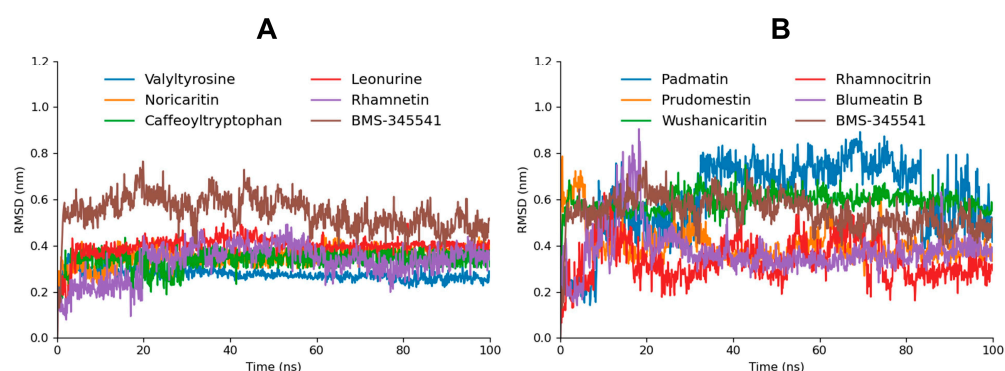


Figure 5. The RMSD graphs of the top five screened compounds compared to BMS-345541 are depicted in graph (A), while the RMSD graphs of the five following top docked compounds compared to BMS-345541 are depicted in graph (B).

In contrast, Padmatin, Rhamnocitrin, and Prudomestine demonstrated highly fluctuating RMSD profiles throughout the simulation, indicating weaker stability and significant structural deviations within the binding pocket. These fluctuations suggest that their initial docking poses were less optimal or that their interactions with the target protein were insufficient to maintain a stable complex. This instability is consistent with their comparatively lower docking scores, highlighting a correlation between binding energy and structural stability during MD simulations.

2.4.2. Hydrogen Bonds

The hydrogen bond plot analysis of the simulated compounds offered deeper insights into their binding interactions and stability during the 100 ns molecular dynamics (MD) simulation [46–48]. Among the screened compounds, Valyltyrosine and Caffeoilytrypto-

phan demonstrated the most stable interaction profiles, forming two consistent actual hydrogen bonds throughout the simulation. Additionally, both compounds exhibited three potential hydrogen bonds, indicating a strong and stable binding affinity with the target protein. These findings align closely with their superior docking scores, further supporting their high binding efficacy and stable conformations under dynamic conditions. Noricaritin, Leonurine, and Rhamnetin, while showing slightly lower stability in their interaction profiles compared to Valyltyrosine and Caffeyltryptophan, maintained an average of one consistent actual hydrogen bond throughout the simulation (Figure 6). Each of these compounds also exhibited a varying number of potential hydrogen bonds, suggesting intermittent but significant interactions within the binding pocket. Notably, Noricaritin's interaction profile is consistent with its high docking score and RMSD stability, highlighting its robustness as a candidate. Leonurine and Rhamnetin, though slightly less stable, still demonstrated meaningful interactions that contribute to their moderate docking scores. BMS-345541, as the reference compound, manifested one interaction in most of the trajectories. Furthermore, the remaining compounds, including Wushanicaritin, Blumeatin B, Padmatin, Rhamnocitrin, and Prudomestin, displayed less consistent hydrogen bond profiles, averaging one or fewer actual hydrogen bonds during the simulation. While these compounds exhibited potential hydrogen bonds, the lack of stable interactions suggests weaker or less reliable binding. This observation aligns with their lower docking scores and fluctuating RMSD values, indicating that their binding modes may not be optimal for sustained interactions.

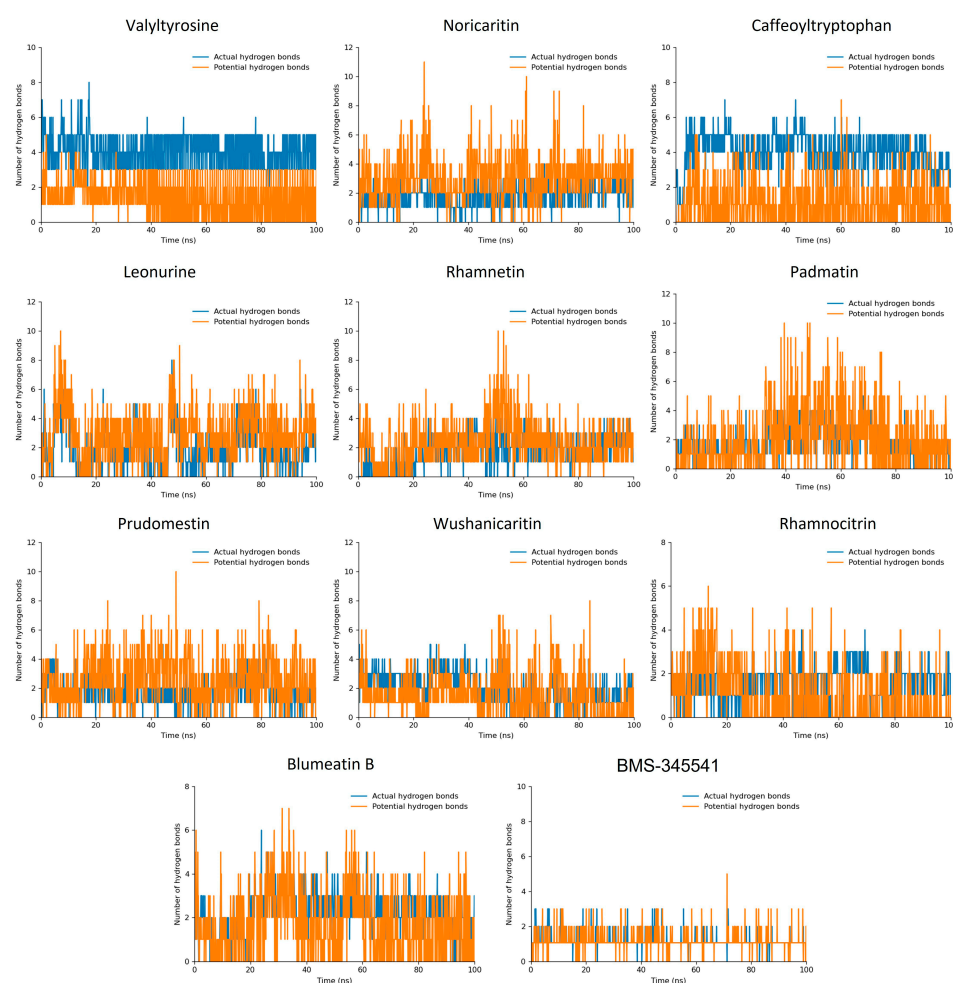


Figure 6. The hydrogen bond plots of the top 10 docked compounds. The blue bar lines highlight the actual hydrogen bonds while the orange bar lines highlight the potential hydrogen bonds.

Comparatively, the stability and number of hydrogen bonds observed in Valyltyrosine and Caffeoilytryptophan underscore their strong potential as lead compounds, as their binding interactions were consistently maintained throughout the MD simulation. Noricaritin stands out among the other compounds for its stable hydrogen bonding and strong correlation with docking scores, making it a promising candidate for further study. In contrast, the weaker and less stable hydrogen bonding profiles of the lower-ranked compounds reinforce their reduced potential for further development. This analysis highlights the importance of stable hydrogen bonding in achieving high binding affinity and stability, providing critical insights into the molecular interactions that govern the efficacy of these compounds.

2.4.3. MD Interaction Energy

The interaction energy analysis, including Coulomb (Coul-SR) and Lennard-Jones (LJ-SR) contributions [49,50], provides a detailed understanding of the binding energetics of the top 10 docked compounds with the target protein. The total interaction energy, derived from the sum of Coul-SR and LJ-SR energies, highlights the stability and strength of these interactions, supporting the findings from molecular docking and MD simulations (Figure 7). Valyltyrosine exhibited the most favorable total interaction energy (-89.16092 kcal/mol), with a significant contribution from Coul-SR energy (-67.9613 kcal/mol) and a moderate LJ-SR component (-21.1996 kcal/mol) as compared to the reference compound BMS-345541 (-48.7817 kcal/mol). These results reflect its strong electrostatic interactions and stable binding within the active site, consistent with its high docking score, stable RMSD profile, and the presence of stable hydrogen bonds during MD simulation. Similarly, Caffeoilytryptophan, with a total interaction energy of -87.0767 kcal/mol, showed a strong Coul-SR energy component (-61.8838 kcal/mol), aligning with its robust binding profile and consistent hydrogen bonding.

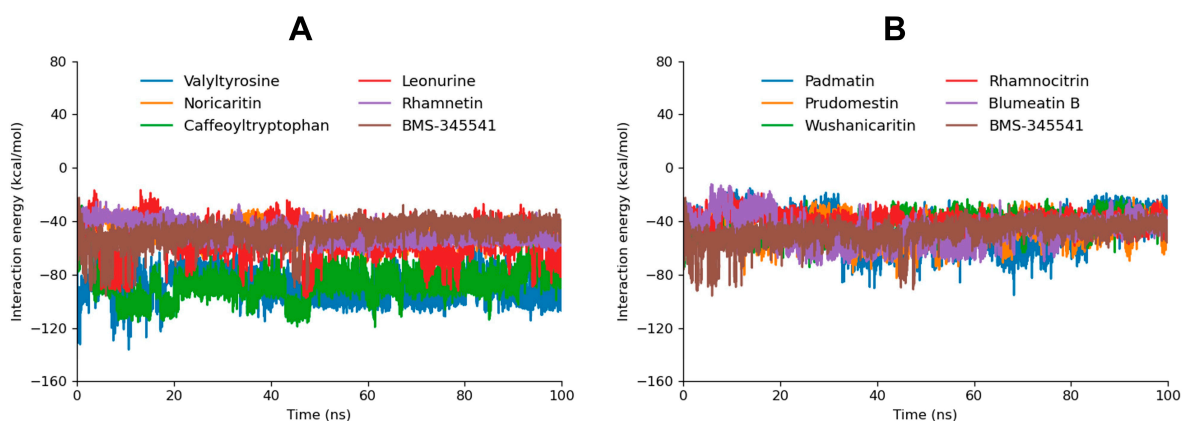


Figure 7. The interaction energy graphs of the top five screened compounds compared to BMS-345541 are depicted in graph (A). Moreover, the interaction energy graph of the five following compounds compared to BMS-345541 are depicted in graph (B).

Noricaritin, Leonurine, and Rhamnetin exhibited moderate total interaction energies (-48.02299 kcal/mol, -55.6563 kcal/mol, and -48.6810 kcal/mol, respectively). The higher LJ-SR contribution in Noricaritin (-32.7132 kcal/mol) and Rhamnetin (-32.2729 kcal/mol) highlights their reliance on van der Waals interactions, which aligns with their moderate docking scores and stable but fewer hydrogen bonds. Leonurine, with a balanced contribution of Coul-SR (-25.9197 kcal/mol) and LJ-SR (-29.7366 kcal/mol) energies (Table 3), exhibited stable RMSD but fewer hydrogen bonds during the MD simulation, consistent with its intermediate interaction profile.

Table 3. The MD interaction energy of the simulated compounds was calculated during the 100 ns MD simulation, representing both Coulombic and Lennard-Jones contributions.

| Sr No | Compound | Interaction Energy (kcal/mol) | | |
|-------|--------------------|-------------------------------|----------|--------------|
| | | Coul-SR | LJ-SR | Total Energy |
| 1 | Valyltyrosine | −67.9613 | −21.1996 | −89.1609 |
| 2 | Noricaritin | −15.3098 | −32.7132 | −48.0230 |
| 3 | Caffeoyltryptophan | −61.8838 | −25.1929 | −87.0767 |
| 4 | Leonurine | −25.9197 | −29.7366 | −55.6563 |
| | BMS-345541 | −22.4512 | −26.3305 | −48.7817 |
| 5 | Rhamnetin | −16.4080 | −32.2729 | −48.6810 |
| 6 | Padmatin | −20.3729 | −25.0026 | −45.3755 |
| 7 | Prudomestin | −17.5392 | −28.8298 | −46.3691 |
| 8 | Wushanicaritin | −13.8759 | −29.9935 | −43.8694 |
| 9 | Rhamnocitrin | −11.7390 | −28.0021 | −39.7412 |
| 10 | Blumeatin B | −22.8464 | −24.3362 | −47.1826 |

Compounds such as Padmatin, Prudomestin, and Wushanicaritin demonstrated slightly weaker total interaction energies (−45.3755 kcal/mol, −46.3691 kcal/mol, and −43.8694 kcal/mol, respectively). These results align with their fluctuating RMSD profiles and fewer stable hydrogen bonds observed during MD simulations, indicating moderate binding affinity. Blumeatin B, while having a lower total interaction energy (−47.1826 kcal/mol), showed a high LJ-SR contribution (−24.3362 kcal/mol) and displayed stabilizing behavior later in the MD simulation, suggesting potential for optimization.

Rhamnocitrin had the weakest total interaction energy (−39.7412 kcal/mol), driven by the lowest Coul-SR component among the compounds. This corresponds to its unstable RMSD profile and fewer hydrogen bonds, confirming its limited binding potential.

2.4.4. MD Simulation Analysis

To evaluate the stability and binding persistence of the top five compounds within the active site of IKK α , snapshots were captured at the 100 ns mark from the molecular dynamics (MD) simulations for each protein-ligand complex. Detailed analysis of these structures revealed that all compounds consistently remained anchored within the active binding pocket throughout the simulation. The presence of stable hydrogen bonds and hydrophobic interactions further confirmed their compatibility and strong binding affinity toward IKK α (Figure 8).

Valyltyrosine and Caffeoyltryptophan consistently emerge as the top-performing compounds across all analyses. Their strong total interaction profile, stable RMSD graph, and robust hydrogen bonding patterns highlight their high binding affinity and dynamic stability, making them the most promising candidates for further exploration. Noricaritin, with a notable reliance on van der Waals interactions, exhibits moderate but consistent performance, aligning well with its intermediate docking score and hydrogen bond stability.

Compounds like Leonurine and Rhamnetin demonstrate a balanced interaction profile, stable RMSD profiles, and moderate hydrogen bonding, positioning them as viable secondary candidates. Overall, the interplay between the docking scores, RMSD stability, hydrogen bond analysis, and interaction profile highlights Valyltyrosine, Caffeoyltryptophan, and Noricaritin as top candidates for further development, while emphasizing the need to refine and optimize lower-ranked compounds.

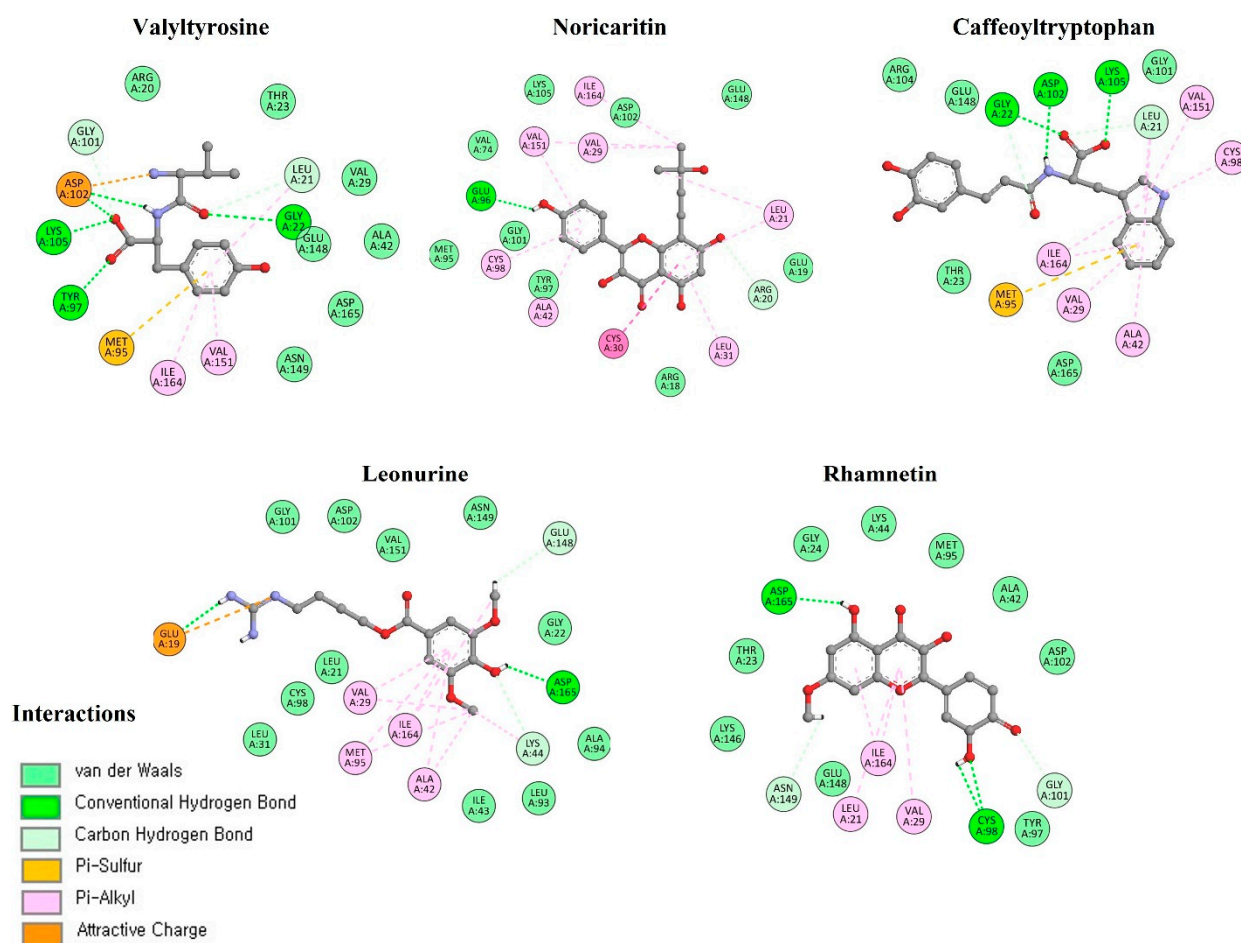


Figure 8. The interaction profile of top candidate compounds at 100 ns MD snapshot.

2.5. Free Energy Calculation

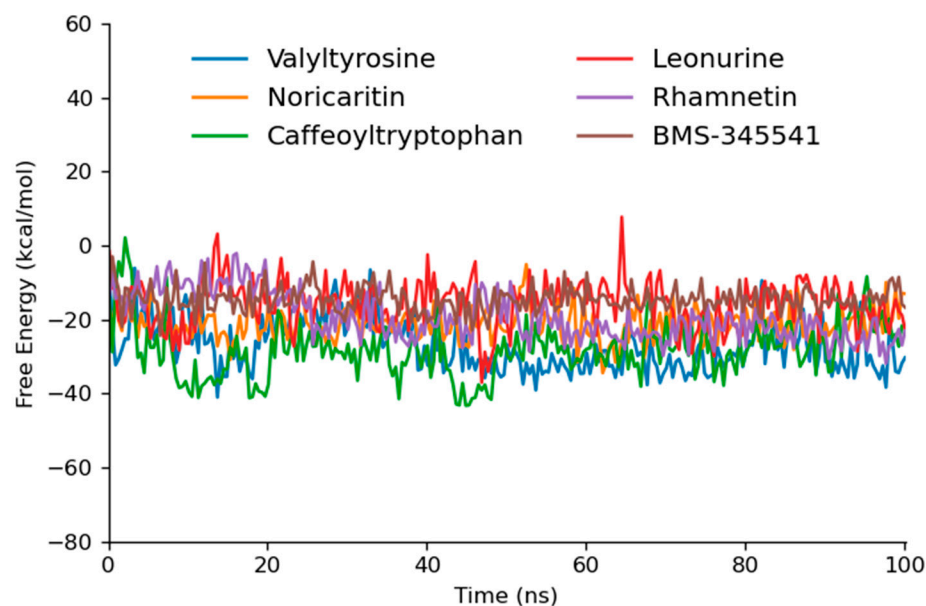
The gmxMMPBSA analysis plays a critical role in molecular dynamics studies by providing a detailed estimation of binding free energies between a ligand and a target protein [51]. It allows the evaluation of the energetics of molecular interactions in a biologically relevant environment. This analysis is essential for understanding the thermodynamic stability of ligand–receptor complexes. By providing a more accurate prediction of binding affinities, gmxMMPBSA helps in identifying potent inhibitors and optimizing lead compounds.

Caffeoyltryptophan exhibited the most favorable ΔG (-28.09 kcal/mol) among the tested and reference compounds, indicating its strong binding affinity and dynamic stability (Table 4). This result is consistent with its high interaction energy during MD simulations, where it demonstrated robust Coulombic and van der Waals interactions, as well as stable hydrogen bonding. Similarly, Valyltyrosine, with a ΔG of -27.07 kcal/mol, showed a comparable thermodynamic profile (Figure 9). Its excellent interaction energy in MD, coupled with consistent RMSD and hydrogen bond stability, underscores its potential as a lead compound.

Noricaritin, with a ΔG of -21.18 kcal/mol and the lowest standard deviation (4.50), exhibited a moderate binding affinity. Its lower thermodynamic stability compared to Caffeoyltryptophan and Valyltyrosine is mirrored in its interaction energy from MD simulations, which showed a higher reliance on van der Waals forces and less pronounced Coulombic interactions. This suggests that while Noricaritin is a strong candidate, its binding may rely on less stable interactions.

Table 4. The calculated gmxMMPBSA free energy of top six screened compounds.

| Sr No | Compounds | $\Delta G_{(TOTAL)}$ | Standard Deviation |
|-------|--------------------|----------------------|--------------------|
| 1 | Valyltyrosine | −27.07 | 6.94 |
| 2 | Noricaritin | −21.18 | 4.50 |
| 3 | Caffeoyltryptophan | −28.09 | 7.25 |
| 4 | Leonurine | −15.74 | 6.38 |
| 5 | Rhamnetin | −19.20 | 6.40 |
| 6 | BMS-345541 | −14.65 | 3.44 |

**Figure 9.** The gmxMMPBSA free energy graphs of the top five docked compounds that performed outstandingly at each step.

Leonurine and Rhamnetin demonstrated less favorable ΔG values of -15.74 kcal/mol and -19.20 kcal/mol, respectively. Both compounds, though displaying meaningful hydrogen bonding and van der Waals interactions, seem to lack the strong Coulombic contributions observed in higher-performing compounds, potentially limiting their overall binding strength.

2.6. Experimental Validation

To validate the computational predictions that these compounds efficiently bind to IKK α , the phosphorylation levels of I κ B α were examined in LPS-stimulated RAW 264.7 cells, as IKK α phosphorylates I κ B α to initiate its proteasomal degradation [52,53]. A significant increase in I κ B α phosphorylation was observed following the LPS treatment, while treatment with BMS-345541, a known IKK α inhibitor, led to a marked reduction in I κ B α phosphorylation levels (Figure 10). The phosphorylation of I κ B α was also attenuated by all tested compounds—Valyltyrosine, Noricaritin, Leonurine, and Caffeoyltryptophan—although their inhibitory effects were less pronounced than those of BMS-345541. Structural modifications may enhance their potency. Interestingly, despite the inhibition of I κ B α degradation, a reduction in total I κ B α levels was also observed. This effect may be attributed to the suppression of NF- κ B-mediated transcriptional feedback, which normally restores I κ B α levels [54–57]. These findings provide experimental validation of the computational predictions and suggest that these compounds could serve as potential IKK α inhibitors for further investigations.

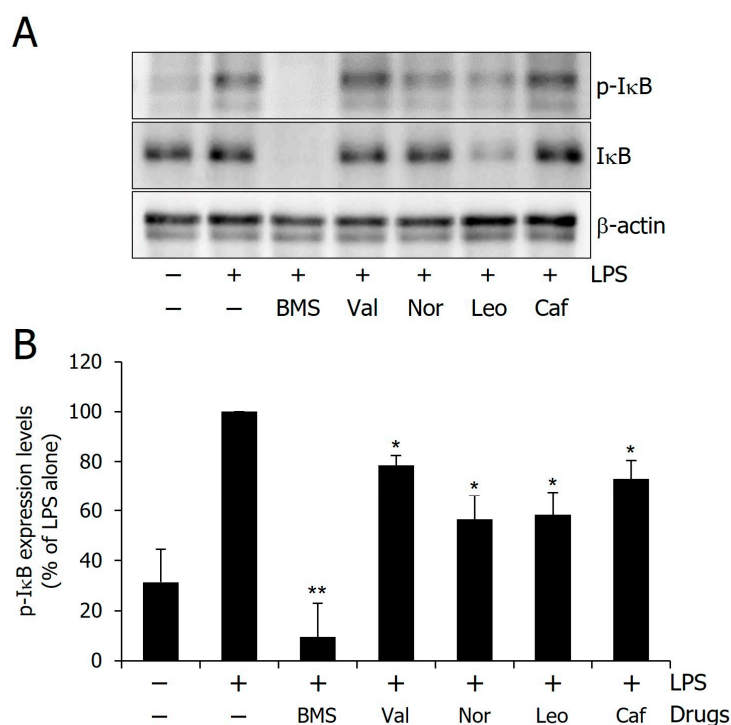


Figure 10. Inhibitory effect of the compounds on the IκBα phosphorylation. (A) Representative western blot image showing IκBα phosphorylation levels. (B) Quantitative analysis of phosphorylation levels. Single (*) and double (**) marks represent statistical significance in $p < 0.05$ and $p < 0.01$, respectively.

A comparative analysis between *in silico* predictions and experimental outcomes underscores the complementarity of these approaches. Valyltyrosine and Caffeylytryptophan, which showed the most favorable profiles in molecular docking, dynamics, and free energy calculations, also demonstrated notable inhibition of IκBα phosphorylation; however, the inhibition was less than expected, thereby validating their predicted binding affinity and stability. Interestingly, Noricaritin and Leonurine, which ranked slightly lower in computational analyses, displayed stronger biological activity than Valyltyrosine. This discrepancy suggests that certain dynamic or cellular factors may influence their *in vitro* performance and are not fully captured by computational models. These findings highlight the importance of combining *in silico* screening with biological validation to more accurately identify and prioritize lead compounds for further optimization.

3. Materials and Methods

3.1. Pharmacophore Modeling and Library Screening

The pharmacophore modeling was employed to generate key interaction features of receptor–ligand binding for the IKKα protein. The crystal structure of IKKα was retrieved from the Protein Data Bank (PDB ID: 5EBZ) to serve as the structural foundation for this analysis. Therefore, the protein kinase domain ranges from 15AA to 302AA was selected; the remaining amino acids were deleted from the data set for more focused analysis. Both the protein kinase domain of IKKα and its co-crystallized ligand were utilized to generate receptor–ligand interaction pharmacophore features using the RLIPG (Receptor–Ligand Interaction Pharmacophore Generation) module in Discovery Studio.

The Receptor–Ligand Interaction Pharmacophore Generation (RLIPG) protocol within Discovery Studio is an advanced tool for constructing pharmacophore models based on receptor–ligand interactions. This protocol offers several key advantages: it operates through a fully automated workflow, efficiently converting receptor–ligand complexes into detailed pharmacophore models; it allows for customizable constraints to precisely

define interaction features between receptors and ligands; and it systematically generates all potential pharmacophore combinations, ranks them based on their selectivity scores, and prioritizes the top-ranked models for further investigation. These capabilities enable precise identification of the key molecular features driving selective binding at the IKK α active site.

3.2. Library Screening

To leverage this pharmacophore model, we utilized a curated natural product library for pharmacophore screening. The library, sourced from the MedChemExpress database (Natural Product Library Plus, catalog number HY-L021P, accessed on 10 October 2024), was selected for its diverse range of bioactive compounds such as 5540 natural products including Phenols (1383), Ketones, Aldehydes, Acids (930), Terpenoids (833), Alkaloids (622), Flavonoids (622), Phenylpropanoids (348), Steroids (277), Saccharides (179), Antibiotics (148), Quinones (100), Amino acids (78), Stilbenes (35), Cyclopeptides (8), Glucosinolates (7), and Others (961).

This library was screened against the pharmacophore model using Discovery Studio's Library Screening tool, ensuring a robust and efficient identification of compounds that matched the pharmacophore features. This methodology enabled us to pinpoint compounds with a high likelihood of selectively interacting with the IKK α binding pocket, with the fit value ranging from 4.6486 to 1.2752×10^{-6} . Out of 5540 compounds, only 82 compounds were screened according to six pharmacophore maximal features. The comprehensive screening process not only ensured high specificity but also facilitated the identification of diverse scaffolds that can be further optimized. By integrating pharmacophore generation and screening with a carefully selected compound library, this study provides a structured approach for the rational discovery of selective inhibitors targeting IKK α .

3.3. Molecular Docking

Molecular docking is a key computational technique used to predict the binding affinity and orientation of ligands within a target protein's active site, based on calculated binding energies of protein–ligand complexes. In this study, the IKK α crystal structure (PDB ID: 5EBZ) was prepared by removing all co-crystallized ligands and water molecules, and hydrogen atoms were added using the receptor preparation tool in Discovery Studio. The CHARMM force field was employed for energy minimization and optimization of the receptor. Ligand structures were processed using the ligand preparation module, which involved generating relevant tautomers and stereoisomers, assigning ionization states at pH 7.4, correcting valence issues, and applying energy minimization using the CHARMM force field. Molecular docking simulations were performed using the CDocker module, a grid-based molecular dynamics (MD) simulated-annealing algorithm that uses CHARMM-based force field parameters to evaluate binding poses. A maximum of 10 poses per ligand was generated, and docking was carried out within a defined binding site radius of 12 Å around the co-crystallized ligand. The docking protocol incorporated default annealing dynamics settings and energy evaluation at the final minimization stage. The resulting protein–ligand complexes were ranked based on CDocker energy and CDocker interaction energy values (in kcal/mol), which represent the internal strain energy and binding strength of the ligand to the receptor, respectively, enabling accurate identification of the most favorable binding conformations.

3.4. Molecular Dynamics Simulations

The top 10 compounds with the lowest docking energies underwent a 100 ns molecular dynamics (MD) simulation to analyze their dynamic stability and interactions with the

target protein. Simulations were set up using CHARMM36 force field parameters generated through the CHARMM-GUI server (<https://www.charmm-gui.org/?doc=input/solution>) (accessed on 2 October 2024), which also provided input files for GROMACS. The system was solvated in a cubic box with the TIP3P water model with a minimum distance of 10 Å between the protein surface and the box edge, neutralized with counter ions, and prepared with periodic boundary conditions.

The key interactions, including electrostatics and van der Waals forces, were calculated using the Verlet method with a 10 Å cutoff radius, while the particle mesh Ewald (PME) method ensured precise electrostatic calculations. Bond lengths were constrained using the LINCS algorithm. The systems underwent energy minimization via the steepest descent method and were equilibrated under NVT and NPT conditions before the production run.

Simulations were executed in GROMACS 2019.3 with a 2fs time step for accurate trajectory sampling. This workflow, supported by CHARMM-GUI scripted file for format conversion, enabled detailed structural and interaction analysis of the protein–ligand complexes, revealing critical insights into their dynamic stability and binding behavior.

3.5. Free Energy Calculation

The gmx_MMPBSA v1.6.3 tool is specifically designed to compute the end-state free energies of protein–ligand complexes using MD trajectory data generated in GROMACS. This tool employs the MM/PBSA (Mechanics/Poisson–Boltzmann Surface Area) method to estimate binding free energies by individually analyzing the protein–ligand complex, the isolated receptor, and the ligand within an explicit solvent environment. The binding free energy ($\Delta G_{\text{binding}}$) of the lead compounds to the target protein was determined using the following equation:

$$\Delta G_{\text{binding}} = G_{\text{complex}} - (G_{\text{protein}} + G_{\text{ligand}}) \quad (1)$$

In this equation, G_{complex} refers to the total energy of the protein–ligand complex, while G_{protein} and G_{ligand} represent the energies of the isolated protein and ligand in a solvated state, respectively.

3.6. Experimental Reagents and Cell Culture

Bacterial lipopolysaccharide (LPS) from *Escherichia coli* serotype 055:B5 was purchased from Sigma-Aldrich (St. Louis, MO, USA). BMS-345541, Valyltyrosine, Noricaritin, Leonurine, and Caffeoyltryptophan were purchased from MedChemExpress (Monmouth Junction, NJ, USA). RAW 264.7 macrophage cells were purchased from the Korea cell line bank (KCLB, cat #40071). RAW 264.7 macrophage cells were maintained in Dulbecco's modified Eagle's medium (DMEM; BYLABS, Luscience Corporation, Hanam-si, Gyeonggi-do, Republic of Korea) containing 10% heat-inactivated fetal bovine serum and 100 U/mL penicillin–streptomycin (Gibco, New York, NY, USA) at 37 °C, 5% CO₂. Cells were incubated in 100 µM of various reagents for 1 h and then stimulated with 1 µg/mL of LPS for 4 h.

3.7. Western Blot Analysis

RAW 264.7 cells were pretreated with 100 µM BMS-345541, Valyltyrosine, Noricaritin, Leonurine, or Caffeoyltryptophan for 1 h prior to stimulation with 1 µg/mL LPS for 4 h. The cells were washed with PBS and lysed in PRO-PREP lysis buffer (iNtRON Biotechnology, Seongnam, Republic of Korea). Equal amounts of protein were separated on 10% SDS-polyacrylamide gel. The proteins were transferred to the Hybond PVDF membrane (Merck KGaA, Darmstadt, Germany) and blocked in 5% skim milk in TBST for 1 h at room temperature. Specific antibodies against p-IkB, IkB (1:1000; Cell signaling

Technology, Danvers, MA, USA), β -actin (1:1000; Santa Cruz Biotechnology Inc., Dallas, TX, USA) were diluted in 5% skim milk. After thoroughly washing with TBST, horseradish peroxidase-conjugated secondary antibodies were applied. The blots were developed by the enhanced chemiluminescence detection (Abfrontier, GW Vieck, Seoul, Republic of Korea). Signals were captured and measured using the FUSION SOLO S imager (VILBER, Collegien, France).

3.8. Statistical Analysis

All values shown in the figures were expressed as the mean \pm SD obtained from three independent experiments. The statistical significance was analyzed by a two-tailed Student's *t*-test. Data with values of $p < 0.05$ were considered statistically significant. Single (*) and double (**) marks represent statistical significance in $p < 0.05$ and $p < 0.01$, respectively.

4. Conclusions

This study highlights the significance of selectively targeting IKK α as a therapeutic approach for cancers and inflammatory diseases driven by dysregulated NF- κ B signaling. A rigorous computational workflow was employed to identify Valyltyrosine and Caffeoily-tryptophan as the most promising candidates based on molecular docking, interaction energy, and free energy calculations. However, despite Valyltyrosine's strong performance in computational analyses, its inhibitory effect on I κ B α phosphorylation in experimental validation was less pronounced than expected. Interestingly, Noricaritin and Leonurine demonstrated notable experimental activity. This suggests that structural modifications to these compounds could further enhance their inhibitory potential. The experimental evaluation conducted in LPS-stimulated RAW 264.7 cells revealed that the selected compounds effectively attenuated I κ B α phosphorylation. However, their inhibitory effects, while significant, were somewhat less pronounced than those of BMS-345541, indicating room for further optimization.

The selective inhibition of IKK α presents a significant therapeutic advantage, particularly in avoiding the adverse effects and toxicity associated with IKK β inhibition, such as inflammatory skin diseases and increased epithelial vulnerability. By focusing on IKK α , this study enhances the understanding of its pivotal role in cancer progression and inflammation while identifying promising lead compounds for targeted therapeutic strategies. The integration of *in silico* and experimental approaches provides a strong foundation for further preclinical development, paving the way for more effective and safer IKK α -targeted therapies.

Supplementary Materials: The following supporting information can be downloaded at: <https://www.mdpi.com/article/10.3390/molecules30092025/s1>, Table S1: The predicted 10 pharmacophore hypotheses; Table S2: The molecular docking scores of all sixty compounds docked against IKK α ; Figure S1: The 2D representation of the interactions of the top5 docked compounds; Figure S2: The 3D interactions images of five compounds following top five; Figure S3: The MD simulation results of the reference compounds IMD-2560 and TPCA1 against IKK α .

Author Contributions: M.Y. and J.P. were involved in the experimental operation and data analysis. E.-T.H., W.S.P. and J.-H.H. were involved in data curation and the methodology. J.C. and W.C. were involved in the conceptualization and writing of the manuscript. M.Y. and W.C. confirmed the authenticity of all the raw data. W.C. was involved in the reviewing and editing of the manuscript. All authors have read and agreed to the published version of the manuscript.

Funding: This work was supported by Korea Basic Science Institute (National Research Facilities and Equipment Center) grants funded by the Ministry of Education (2022R1A6C101A739, W.C.; 2020R1A6C101A195, J.C.).

Institutional Review Board Statement: Not applicable.

Informed Consent Statement: Not applicable.

Data Availability Statement: The data that support the findings of this study are available from the corresponding author upon reasonable request.

Acknowledgments: W.C. and J.C. acknowledge the Research Grants from the National Research Foundation of Korea.

Conflicts of Interest: The authors declare that they have no competing interests.

References

1. Puar, Y.R.; Shanmugam, M.K.; Fan, L.; Arfuso, F.; Sethi, G.; Tergaonkar, V.J.B. Evidence for the involvement of the master transcription factor NF- κ B in cancer initiation and progression. *Biomedicines* **2018**, *6*, 82. [\[CrossRef\]](#)
2. Khan, A.; Zhang, Y.; Ma, N.; Shi, J.; Hou, Y.J.C.G.T. NF- κ B role on tumor proliferation, migration, invasion and immune escape. *Cancer Gene Ther.* **2024**, *31*, 1599–1610. [\[CrossRef\]](#)
3. Deka, K.; Li, Y.J.C. Transcriptional regulation during aberrant activation of NF- κ B signalling in cancer. *Cells* **2023**, *12*, 788. [\[CrossRef\]](#)
4. Lin, Y.; Bai, L.; Chen, W.; Xu, S. The NF- κ B activation pathways, emerging molecular targets for cancer prevention and therapy. *Expert Opin. Ther. Targets* **2010**, *14*, 45–55. [\[CrossRef\]](#)
5. Li, Y.; Zhao, B.; Peng, J.; Tang, H.; Wang, S.; Peng, S.; Ye, F.; Wang, J.; Ouyang, K.; Li, J.; et al. Inhibition of NF- κ B signaling unveils novel strategies to overcome drug resistance in cancers. *Drug Resist. Updates* **2024**, *73*, 101042. [\[CrossRef\]](#)
6. Pavitra, E.; Kancharla, J.; Gupta, V.K.; Prasad, K.; Sung, J.Y.; Kim, J.; Tej, M.B.; Choi, R.; Lee, J.-H.; Han, Y.-K.; et al. The role of NF- κ B in breast cancer initiation, growth, metastasis, and resistance to chemotherapy. *Biomed Pharmacother.* **2023**, *163*, 114822. [\[CrossRef\]](#)
7. Xia, L.; Tan, S.; Zhou, Y.; Lin, J.; Wang, H.; Oyang, L.; Tian, Y.; Liu, L.; Su, M.; Wang, H.; et al. Role of the NF κ B-signaling pathway in cancer. *Onco Targets Ther.* **2018**, *11*, 2063–2073. [\[CrossRef\]](#)
8. Singh, A.P.; Sharma, A.K.; Singh, T.G. Unlocking the Therapeutic Potential: Exploring nf- κ b as a Viable Target for Diverse Pharmacological Approaches. *Int. J. Pharm. Pharm. Sci.* **2024**, *16*, 1–9. [\[CrossRef\]](#)
9. Oh, A.; Pardo, M.; Rodriguez, A.; Yu, C.; Nguyen, L.; Liang, O.; Chorzalska, A.; Dubielecka, P.M. NF- κ B signaling in neoplastic transition from epithelial to mesenchymal phenotype. *Cell Commun. Signal.* **2023**, *21*, 291. [\[CrossRef\]](#)
10. Huang, W.-C.; Hung, M.-C. Beyond NF- κ B activation: Nuclear functions of I κ B kinase α . *J. Biomed. Sci.* **2013**, *20*, 3. [\[CrossRef\]](#)
11. Kanarek, N.; Ben-Neriah, Y. Regulation of NF- κ B by ubiquitination and degradation of the I κ Bs. *Immunol. Rev.* **2012**, *246*, 77–94. [\[CrossRef\]](#)
12. Chen, Z.J. Ubiquitination in signaling to and activation of IKK. *Immunol Rev.* **2012**, *246*, 95–106. [\[CrossRef\]](#)
13. Kanarek, N.; London, N.; Schueler-Furman, O.; Ben-Neriah, Y. Ubiquitination and degradation of the inhibitors of NF- κ B. *Cold Spring Harb. Perspect. Biol.* **2010**, *2*, a000166. [\[CrossRef\]](#)
14. Ghosh, S.; Dass, J.F.P. Study of pathway cross-talk interactions with NF- κ B leading to its activation via ubiquitination or phosphorylation: A brief review. *Gene* **2016**, *584*, 97–109. [\[CrossRef\]](#)
15. Mitchell, S.; Vargas, J.; Hoffmann, A. Medicine, Signaling via the NF κ B system. *Wiley Interdiscip Rev. Syst. Biol. Med.* **2016**, *8*, 227–241. [\[CrossRef\]](#)
16. Vu, D.; Huang, D.-B.; Vemu, A.; Ghosh, G. A structural basis for selective dimerization by NF- κ B RelB. *J. Mol. Biol.* **2013**, *425*, 1934–1945. [\[CrossRef\]](#)
17. Sun, S.C. The noncanonical NF- κ B pathway. *Immunol Rev.* **2012**, *246*, 125–140. [\[CrossRef\]](#)
18. Lovas, A.; Weidemann, A.; Albrecht, D.; Wiechert, L.; Weih, D.; Weih, F. p100 Deficiency is insufficient for full activation of the alternative NF- κ B pathway: TNF cooperates with p52-RelB in target gene transcription. *PLoS ONE* **2012**, *7*, e42741. [\[CrossRef\]](#)
19. de Oliveira, K.A.; Kaergel, E.; Heinig, M.; Fontaine, J.-F.; Patone, G.; Muro, E.M.; Mathas, S.; Hummel, M.; Andrade-Navarro, M.A.; Hübner, N.; et al. A roadmap of constitutive NF- κ B activity in Hodgkin lymphoma: Dominant roles of p50 and p52 revealed by genome-wide analyses. *Genome Med.* **2016**, *8*, 28. [\[CrossRef\]](#)
20. Chatterjee, B.; Roy, P.; Sarkar, U.A.; Zhao, M.; Ratra, Y.; Singh, A.; Chawla, M.; De, S.; Gomes, J.; Sen, R.; et al. Immune differentiation regulator p100 tunes NF- κ B responses to TNF. *Front. Immunol.* **2019**, *10*, 997. [\[CrossRef\]](#)
21. Giridharan, S.; Srinivasan, M. Mechanisms of NF- κ B p65 and strategies for therapeutic manipulation. *J. Inflamm. Res.* **2018**, *ume* *11*, 407–419. [\[CrossRef\]](#)
22. Chawla, M.; Roy, P.; Basak, S. Role of the NF- κ B system in context-specific tuning of the inflammatory gene response. *Curr. Opin. Immunol.* **2021**, *68*, 21–27. [\[CrossRef\]](#)

23. Fusco, A.J.; Mazumder, A.; Wang, V.Y.-F.; Tao, Z.; Ware, C.; Ghosh, G. The NF- κ B subunit RelB controls p100 processing by competing with the kinases NIK and IKK1 for binding to p100. *Sci. Signal.* **2016**, *9*, ra96. [\[CrossRef\]](#)
24. Prescott, J.A.; Cook, S.J. Targeting IKK β in cancer: Challenges and opportunities for the therapeutic utilisation of IKK β inhibitors. *Cells* **2018**, *7*, 115. [\[CrossRef\]](#)
25. Llona-Minguez, S.; Baiget, J.; Mackay, S.P. Small-molecule inhibitors of I κ B kinase (IKK) and IKK-related kinases. *Pharm. Pat. Anal.* **2013**, *2*, 481–498. [\[CrossRef\]](#)
26. Liu, F.; Xia, Y.; Parker, A.S.; Verma, I.M. IKK biology. *Immunol. Rev.* **2012**, *246*, 239–253. [\[CrossRef\]](#)
27. Paul, A.; Edwards, J.; Pepper, C.; Mackay, S. Inhibitory- κ B kinase (IKK) α and nuclear factor- κ B (NF κ B)-inducing kinase (NIK) as anti-cancer drug targets. *Cells* **2018**, *7*, 176. [\[CrossRef\]](#)
28. Huang, J.-J.; Chu, H.-X.; Jiang, Z.-Y.; Zhang, X.-J.; Sun, H.-P.; You, Q.-D. Recent advances in the structure-based and ligand-based design of IKK β inhibitors as anti-inflammation and anti-cancer agents. *Curr. Med. Chem.* **2014**, *21*, 3893–3917. [\[CrossRef\]](#)
29. Pasparakis, M. Role of NF- κ B in epithelial biology. *Immunol. Rev.* **2012**, *246*, 346–358. [\[CrossRef\]](#)
30. Mukherjee, T.; Kumar, N.; Chawla, M.; Philpott, D.J.; Basak, S. The NF- κ B signaling system in the immunopathogenesis of inflammatory bowel disease. *Sci. Signal.* **2024**, *17*, eadh1641. [\[CrossRef\]](#)
31. Ito, M.; Hamano, T.; Komatsu, T.; Asamitsu, K.; Yamakawa, T.; Okamoto, T. A novel IKK α inhibitor, noraristeromycin, blocks the chronic inflammation associated with collagen-induced arthritis in mice. *Mod. Rheumatol.* **2014**, *24*, 775–780. [\[CrossRef\]](#)
32. Anthony, N.G.; Baiget, J.; Berretta, G.; Boyd, M.; Breen, D.; Edwards, J.; Gamble, C.; Gray, A.I.; Harvey, A.L.; Hatzierieremia, S.; et al. Inhibitory kappa B kinase α (IKK α) inhibitors that recapitulate their selectivity in cells against isoform-related biomarkers. *J. Med. Chem.* **2017**, *60*, 7043–7066. [\[CrossRef\]](#)
33. Göktuna, S.I.; Diamanti, M.A.; Chau, T.L. IKKs and tumor cell plasticity. *FEBS J.* **2018**, *285*, 2161–2181. [\[CrossRef\]](#) [\[PubMed\]](#)
34. Anighoro, A.; Bajorath, J.; Rastelli, G. Polypharmacology: Challenges and opportunities in drug discovery: Miniperspective. *J. Med. Chem.* **2014**, *57*, 7874–7887. [\[CrossRef\]](#) [\[PubMed\]](#)
35. Dantas, R.F.; Evangelista, T.C.S.; Neves, B.J.; Senger, M.R.; Andrade, C.H.; Ferreira, S.B.; Silva-Junior, F.P. Dealing with frequent hitters in drug discovery: A multidisciplinary view on the issue of filtering compounds on biological screenings. *Expert Opin. Drug Discov.* **2019**, *14*, 1269–1282. [\[CrossRef\]](#) [\[PubMed\]](#)
36. Horvath, D. Pharmacophore-based virtual screening. *Methods Mol. Biol.* **2011**, *672*, 261–298. [\[PubMed\]](#)
37. Kaserer, T.; Beck, K.R.; Akram, M.; Odermatt, A.; Schuster, D. Pharmacophore models and pharmacophore-based virtual screening: Concepts and applications exemplified on hydroxysteroid dehydrogenases. *Molecules* **2015**, *20*, 22799–22832. [\[CrossRef\]](#)
38. Yasir, M.; Park, J.; Han, E.-T.; Han, J.-H.; Park, W.S.; Chun, W. Identification of Malaria-Selective Proteasome β 5 Inhibitors Through Pharmacophore Modeling, Molecular Docking, and Molecular Dynamics Simulation. *Int. J. Mol. Sci.* **2024**, *25*, 11881. [\[CrossRef\]](#)
39. Li, L.; Gong, S. The discovery of a novel I κ B kinase β inhibitor based on pharmacophore modeling, virtual screening and biological evaluation. *Future Med. Chem.* **2024**, *16*, 531–544. [\[CrossRef\]](#)
40. Sun, H.-P.; Zhu, J.; Chen, F.-H.; Zhang, S.-L.; Zhang, Y.; You, Q.-D. Combination of pharmacophore model development and binding mode analyses: Identification of ligand features essential for I κ B kinase-beta (IKK β) inhibitors and virtual screening based on it. *Eur. J. Med. Chem.* **2011**, *46*, 3942–3952. [\[CrossRef\]](#)
41. Patil, R.; Das, S.; Stanley, A.; Yadav, L.; Sudhakar, A.; Varma, A.K. Optimized hydrophobic interactions and hydrogen bonding at the target-ligand interface leads the pathways of drug-designing. *PLoS ONE* **2010**, *5*, e12029. [\[CrossRef\]](#)
42. Lin, F.-Y.; MacKerell, A.D., Jr. Do halogen-hydrogen bond donor interactions dominate the favorable contribution of halogens to ligand-protein binding? *J. Phys. Chem.* **2017**, *121*, 6813–6821. [\[CrossRef\]](#) [\[PubMed\]](#)
43. Yasir, M.; Park, J.; Han, E.-T.; Park, W.S.; Han, J.-H.; Chun, W. Drug Repositioning via Graph Neural Networks: Identifying Novel JAK2 Inhibitors from FDA-Approved Drugs through Molecular Docking and Biological Validation. *Molecules* **2024**, *29*, 1363. [\[CrossRef\]](#) [\[PubMed\]](#)
44. Yasir, M.; Park, J.; Chun, W. Discovery of Novel Aldose Reductase Inhibitors via the Integration of Ligand-Based and Structure-Based Virtual Screening with Experimental Validation. *ACS Omega* **2024**, *9*, 20338–20349. [\[CrossRef\]](#)
45. Yasir, M.; Park, J.; Han, E.-T.; Park, W.S.; Han, J.-H.; Chun, W. Identification of Potential Trypsin Inhibitors from FDA-Approved Drugs Using Machine Learning, Molecular Docking, and Experimental Validation. *ACS Omega* **2024**, *9*, 38820–38831. [\[CrossRef\]](#)
46. Yasir, M.; Park, J.; Han, E.-T.; Han, J.-H.; Park, W.S.; Chun, W. Investigating the Inhibitory Potential of Flavonoids against Aldose Reductase: Insights from Molecular Docking, Dynamics Simulations, and gmx_MMPBSA Analysis. *Curr. Issues Mol. Biol.* **2024**, *46*, 11503–11518. [\[CrossRef\]](#) [\[PubMed\]](#)
47. Yasir, M.; Park, J.; Han, E.-T.; Han, J.-H.; Park, W.S.; Choe, J.; Chun, W. Identification of Marine Compounds Inhibiting NF- κ B-Inducing Kinase Through Molecular Docking and Molecular Dynamics Simulations. *Biomolecules* **2024**, *14*, 1490. [\[CrossRef\]](#)
48. Liu, X.; Shi, D.; Zhou, S.; Liu, H.; Yao, X. Molecular dynamics simulations and novel drug discovery. *Expert Opin. Drug Discov.* **2018**, *13*, 23–37. [\[CrossRef\]](#)

49. Oliveira, M.P.; Hünenberger, P.H. Influence of the Lennard-Jones Combination Rules on the Simulated Properties of Organic Liquids at Optimal Force-Field Parametrization. *J. Chem. Theory Comput.* **2023**, *19*, 2048–2063. [[CrossRef](#)]
50. Galano-Frutos, J.J.; Sancho, J. Energy, water, and protein folding: A molecular dynamics-based quantitative inventory of molecular interactions and forces that make proteins stable. *Protein Sci.* **2024**, *33*, e4905. [[CrossRef](#)]
51. Valdés-Tresanco, M.S.; Valdés-Tresanco, M.E.; Valiente, P.A.; Moreno, E. gmx_MMPBSA: A New Tool to Perform End-State Free Energy Calculations with GROMACS. *J. Chem. Theory Comput.* **2021**, *17*, 6281–6291. [[CrossRef](#)] [[PubMed](#)]
52. Jang, S.I.; Kim, H.J.; Kim, Y.J.; Jeong, S.I.; You, Y.O. Tanshinone IIA inhibits LPS-induced NF-kappaB activation in RAW 264.7 cells: Possible involvement of the NIK-IKK, ERK1/2, p38 and JNK pathways. *Eur. J. Pharmacol.* **2006**, *542*, 1–7. [[CrossRef](#)]
53. Ku, K.T.; Huang, Y.L.; Huang, Y.J.; Chiou, W.F. Miyabenol A inhibits LPS-induced NO production via IKK/IkappaB inactivation in RAW 264.7 macrophages: Possible involvement of the p38 and PI3K pathways. *J. Agric. Food Chem.* **2008**, *56*, 8911–8918. [[CrossRef](#)] [[PubMed](#)]
54. Hoffmann, A.; Levchenko, A.; Scott, M.L.; Baltimore, D. The IkappaB-NF-kappaB signaling module: Temporal control and selective gene activation. *Science* **2002**, *298*, 1241–1245. [[CrossRef](#)]
55. Covert, M.W.; Leung, T.H.; Gaston, J.E.; Baltimore, D. Achieving stability of lipopolysaccharide-induced NF-kappaB activation. *Science* **2005**, *309*, 1854–1857. [[CrossRef](#)] [[PubMed](#)]
56. Burke, J.R.; Pattoli, M.A.; Gregor, K.R.; Brassil, P.J.; MacMaster, J.F.; McIntyre, K.W.; Yang, X.; Iotzova, V.S.; Clarke, W.; Strnad, J.; et al. BMS-345541 is a highly selective inhibitor of I kappa B kinase that binds at an allosteric site of the enzyme and blocks NF-kappa B-dependent transcription in mice. *J. Biol. Chem.* **2003**, *278*, 1450–1456. [[CrossRef](#)]
57. Karin, M.; Ben-Neriah, Y. Phosphorylation meets ubiquitination: The control of NF-κB activity. *Ann. Rev. Immunol.* **2000**, *18*, 621–663. [[CrossRef](#)]

Disclaimer/Publisher’s Note: The statements, opinions and data contained in all publications are solely those of the individual author(s) and contributor(s) and not of MDPI and/or the editor(s). MDPI and/or the editor(s) disclaim responsibility for any injury to people or property resulting from any ideas, methods, instructions or products referred to in the content.